Electrical Engineering (2022) 104:13–25
https://doi.org/10.1007/s00202-020-01191-4

ORIGINAL PAPER

Design of a master power factor controller for an industrial plant with solar photovoltaic and electric vehicle chargers

Affiq A. Ghani[1] · **Vigna K. Ramachandaramurthy**[1] · **Jia Ying Yong**[1]

Received: 13 July 2020 / Accepted: 9 December 2020 / Published online: 9 February 2021

Abstract

The power factor of industrial facilities is typically inductive. The case study in this paper was based on a typical Malaysian 11-kV on-grid industrial system with renewable energy sources and electric vehicle charging station connected. The integration of renewable energy sources reduces energy consumption from the grid; it consecutively reduces greenhouse gas emissions. However, the integration of renewable energy sources such as solar photovoltaic operating at unity power factor results in a reduction of the industry's power factor. According to the Malaysian Distribution Code, the power factor of a medium voltage industrial system should be more than 0.85 lagging. A long-term low power factor will reduce the related electrical equipment lifespan and increase the monthly electricity bills. A classic method to overcome this issue was by installing reactive power compensator devices, such as the synchronous condenser, static VAr compensator and static synchronous compensator. Studies had revealed that solar photovoltaic with appropriate control system design could perform short-term reactive power compensation. The control techniques used are either power factor control, active power control, reactive power control or any combination of them. However, neither the reactive power compensator devices nor the solar photovoltaic with a control system can regulate the industry's power factor to an intended value throughout its operation. Thus, this paper presents a simple, relatively cost-effective design of a master power factor controller that is capable of regulating the industry's power factor to an intended value throughout its operation with a single preset reference. In this research, an industry-grade system comprises an industrial load installed with a power factor-controlled capacitor bank, a power factor-controlled solar photovoltaic system, a bidirectional current-controlled electric vehicle charging system based on CHAdeMO 1.1 standard charging protocol and a master power factor controller was designed using the Matrix Laboratory/Simulink software. This paper has provided simulation results as proof that each of the designed equipment was functioning appropriately. The results also proved that the proposed master power factor controller was capable of regulating the power factor of the industrial system to above 0.85 lagging throughout its operation.

Keywords *Bidirectional converter · Electric vehicle · Power factor controller · Reactive power compensation · Solar photovoltaic*

Abbreviations

$\alpha\beta$	Alpha–beta frame-based
abc	Abc frame-based
AC	Alternating current
ANSI	American national standard institute
C_{bank}	Capacitor bank
$C_{bankneed}$	Capacitor bank needed to operate to achieve power factor reference of the industrial load
C_{dclink}	DC link capacitor
C_{filter}	Capacitor of the LC filter
CT	Current transformer
D	Discharging
DC	Direct current
D_{con}	Duty ratio of the DC/DC converter
dq	Direct quadrature frame-based
EV	Electric vehicle
f_c	Cut-off frequency
f_s	System frequency
f_{sw}	Switching frequency
I	Current

✉ Affiq A. Ghani
affiqaghani@yahoo.com

[1] Institute of Power Engineering, Department of Electrical Power Engineering, College of Engineering, Jalan IKRAM-UNITEN, Universiti Tenaga Nasional (UNITEN), 43000 Kajang, Selangor, Malaysia

I_{abc}	Three-phase phase-to-ground current
ICEV	Internal combustion engine vehicle
I_d	Current direct
$I_{dcontrol}$	Current direct control
I_{dref}	Current direct reference
IEEE	Institute of electrical and electronics engineers
I_{EV}	Current flow in the electric vehicle charger
I_{Lmax}	Maximum root-mean-square current of the load
I_q	Current quadrature
$I_{qcontrol}$	Current quadrature control
I_{qref}	Current quadrature reference
I_{refEV}	Current reference for the electric vehicle charging system
k	Constant value
K_I	Integral gain
K_P	Proportional gain
L_{filter}	Inductor of the LC filter
Li-Ion	Lithium-ion
MPPT	Maximum power point tracker
NEM	Net energy metering
P	Active power
P_{abcPV}	Three-phase active power output from the solar photovoltaic system
PF	Power factor
PF_{ind}	Power factor of the industrial system
PF_{load}	Power factor of the industrial load
PF_{mref}	Master power factor reference
PF_{needPV}	Power factor needed for the solar photovoltaic system to achieve master power factor reference
PF_{refEV}	Power factor reference for the electric vehicle charging system
$PF_{reflimitPV}$	Limit power factor reference for the solar photovoltaic system
$PF_{refload}$	Power factor reference for the industrial load
PF_{refPV}	Power factor reference for the solar photovoltaic system
P_{ind}	Overall active power received by the industrial system
PLL	Phase-locked loop
P_{maxPV}	Maximum active power output from the solar photovoltaic system
P_{PV}	Active power output from the solar photovoltaic system
PV	Photovoltaic
Q	Reactive power
Q_{ind}	Overall reactive power received by the industrial system
Q_{max}	Maximum reactive power output
Q_{maxPV}	Maximum reactive power output from the solar photovoltaic system
Q_{need}	Reactive power needed to achieve master power factor reference
Q_{PV}	Reactive power output from the solar photovoltaic system
R	Resistance
RES	Renewable energy sources
S	Three-phase apparent power
SPWM	Sine pulse width modulation
SVC	Static VAr compensator
THD_i	Total harmonic distortion of an output current signal
Tx	Transformer
U_{grid}	Voltage at the grid side
U_{nit}	Voltage at the inverter output
V_{dclink}	Direct current link voltage
$V_{dclinkref}$	Direct current link voltage reference
V_{gabc}	Three-phase voltage at the grid side of the industrial system
V_{MPP}	Maximum power point voltage
V_S	Direct current supply voltage
VT	Voltage transformer
X	Reactance
X_C	Capacitor reactance
Z	Impedance

1 Introduction

The electrification of the transportation sector is significantly contributing to a lesser carbon footprint [1]. The sales of electric vehicles (EVs) are increasing, where more on-road EVs are predicted in the foreseeable future [2]. The twenty-first century saw the rapid development of EV technology, where some EVs were shown to have a better performance than regular internal combustion engine vehicles (ICEVs) in terms of energy conversion efficiency, maximum torque and distance covered per full charge [3]. Hence, the projection of EV to replace the ICEV in the nearest future is quite inevitable [4]. In Malaysia, the National Automotive Policy had distributed soft loans amounting to RM 100 million per year to the EVs vendor for installing and developing advanced EV technology and machinery [5].

Meanwhile, the International Energy Agency had reported that, in the most recent time, the industrial sector has the highest electricity consumption worldwide [6]. Fortunately, the adoption of renewable energy sources (RES) has slowly reduced the world's dependency on fuel-based electric generators. The deployment of distributed solar photovoltaic (PV) systems is growing exponentially over the last decade [7]. Many countries have started promoting rooftop solar PV for homes, commercial buildings and industry [8]. The Sustainable Energy Development Authority, a statutory body in Malaysia, had introduced several solar PV policies,

such as Feed-in-Tariff, Self-Consumption and Net Energy Metering (NEM) for residential, commercial, agricultural and industrial sectors [9]. The NEM is a scheme that consumes the electrical energy produced by the solar PV system and exports any excess to the distribution licensees. The installation of solar PV can provide a long-term investment.

Unfortunately, the pure RES installation can cause the power factor (*PF*) at the industry's incomer (PF_{ind}) to reduce drastically. The minimum PF_{ind} value stipulated by the electrical utility in Malaysia is 0.85 lagging [10]. A PF_{ind} lower than that will result in a greater power loss where it leads to equipment overloads, equipment overheating and a shorter service life [11]. So, if the owner of the industry fails to fulfill the regulation, the utility will penalize them with a higher monthly electricity bill [10]. Due to this reason, a need to install a master *PF* controller to regulate the PF_{ind} to an intended value without additional installed equipment is imperative.

The literature in [12] had mentioned installing reactive power (*Q*) compensating devices such as the synchronous condenser, static VAr compensator (SVC) and static synchronous compensator to solve low PF_{ind}. Authors in [13] proposed the hybrid control strategies of SVC for *Q* compensation. However, the authors further added that maintenance is difficult and expensive. Another study in [14] had discussed in-depth the power factor (*PF*), active power (*P*) and *Q* control techniques used in the solar PV system. The control techniques are designed with either quadrature frame-based (*dq*), alpha–beta frame-based ($\alpha\beta$) or *abc* frame-based (*abc*) structures. Authors in [15] had listed five control techniques used for *Q* management in the RES system, namely sliding mode control, model predictive control, soft computing methods, droop speed control and current mode control. The soft computing method has the fastest response speed among all these control techniques, but its algorithm is rather complicated. Elsewhere, a reliable and flexible bidirectional EV charging system with multi-controller was designed [16], where it can perform discharging control (*D*-control), current control (*I*-control), voltage control (*V*-control), *Q*-control and *PF*-control. However, the *Q* compensating devices and controllers mentioned in [12–14, 16] are incapable of regulating PF_{ind} to attain an intended value throughout its operation, and the control techniques mentioned in [15] are complex, correspondingly expensive.

This paper proposes a master *PF* controller that can regulate the PF_{ind} to attain the desired value by a single preset reference throughout its operation. This case study involves the operation of a medium voltage industrial system comprising an 11-kV industrial load with C_{bank}, *PF*-controlled 400 kW_{pk} solar PV system, bidirectional *I*-controlled EV fast-charging system and a master *PF* controller to coordinate them all. This paper discusses the details of each equipment design and control processes involved. The key contributions of this paper are (1) the design of the master *PF* controller which encompass RES, EV and C_{bank} to regulate the PF_{ind} to any preset reference value, (2) the mathematical formula for calculating the C_{dclink} and LC filter sizing and (3) validation of the robustness of the master *PF* controller.

2 Systems modeling

2.1 Overview of the industrial plant

This case study was formulated based on a typical Malaysian 11-kV industrial system integrated with a *PF*-controlled 400 kW_{pk} solar PV system and a bidirectional *I*-controlled EV fast-charging system with three charging ports. The ANSI/IEEE 1585–2002 standard stated that 11-kV is a medium level voltage [17], used in industrial facilities with their step-down transformers for connecting to low-rated voltage systems. In this case study, the installation utilized an 11-kV/400 V transformer for connecting to the solar PV system and EV charging system. The EV model used is the Nissan LEAF 2019, which is powered by lithium-ion (Li-Ion) battery with a capacity of 40 kWh, 114.3 Ah and a nominal voltage of 350.4 V [18]. There are three EVs in total, which act as flexible and dynamic loads. Each of them receives approximately 50 kW with 125 A current transfer during charge mode [19]. The case study in this paper only focuses on charge mode. The proposed master *PF* controller was connected to the industry's current transformer (CT), voltage transformer (VT) and the *PF*-controlled DC/AC converter of the solar PV system. Figure 1a, b illustrates a general diagram of the industrial system and a detailed framework of the interconnection of RES and EV, respectively [20].

For the base case in this research, the industrial load has an unimproved *PF* (PF_{load}) of 0.8 lagging. It was then installed with C_{bank} to ensure that the PF_{ind} is maintained at 0.95 lagging. Next, the industrial system was connected to the solar PV system operating at unity *PF* and the EV charging system where it causes further reduction and alternation in $PF_{ind,}$ respectively. Finally, the industrial system was installed with the proposed master *PF* controller to regulate the PF_{ind} at 0.95 lagging by utilizing the *PF*-controlled solar PV system for *Q* support. The master *PF* controller sends a dynamic control signal to the *PF*-controlled solar PV system as its instantaneous *PF* reference (PF_{refPV}) during the controlling process. A detailed explanation of the proposed control algorithm is given in the control section.

2.2 Capacitor bank control

The capacitor bank (C_{bank}) with a control system [21] is reliable and capable of regulating PF_{ind} to an intended value.

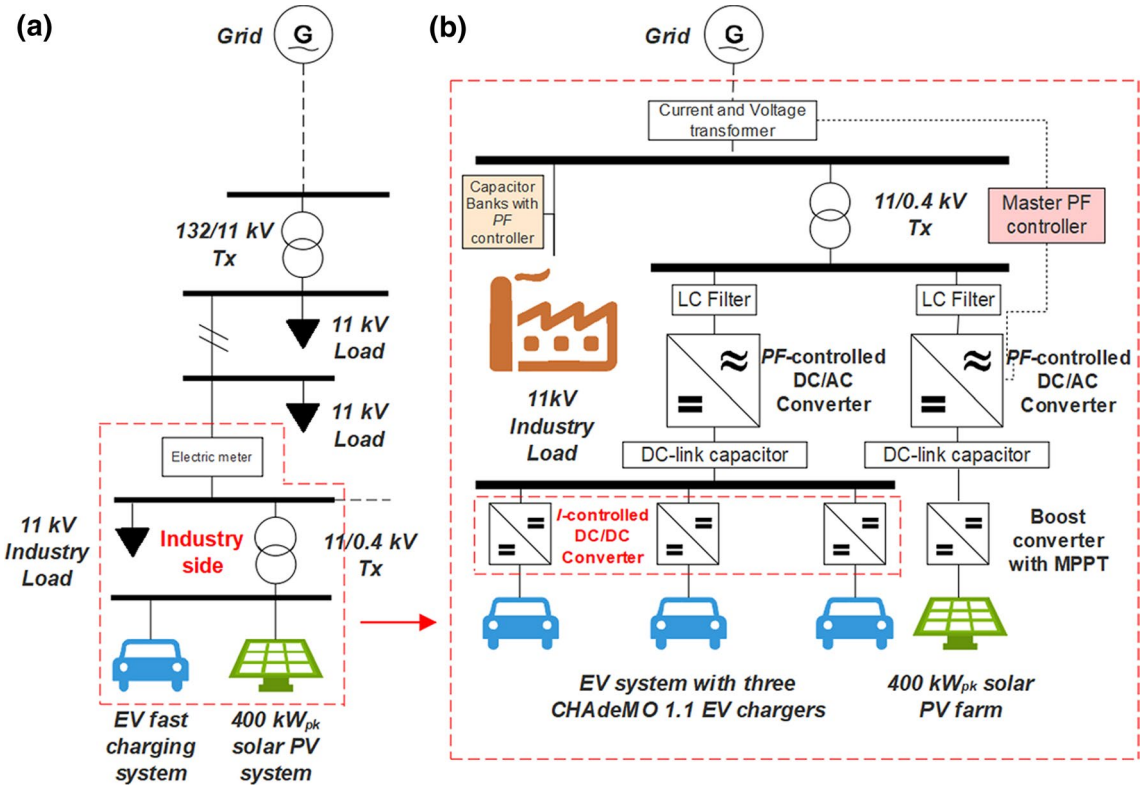

Fig. 1 **a** General diagram of the designed industrial system. **b** A detailed framework of the designed industrial system

The size of the C_{bank} varies according to the load and the intended PF [22]. The industrial load was installed with a 600 kVAr C_{bank} to improve the PF_{ind} from 0.8 lagging to 0.95 lagging. The industrial load reference ($PF_{refload}$) was set to 0.95 lagging because it is more than 0.85 lagging and includes an additional safety margin. The designed C_{bank} comprises thirty fixed stackable and switchable 20 kVAr capacitors. The amount of Q needed to attain $PF_{refload}$, and the number of 20 kVAr capacitors that need to be operated ($C_{bankneed}$) is the base calculation of this PF control. A too large and fixed capacitor size was not preferred as it can cause the PF_{ind} to be in over and under correction [23]. Figure 2 shows the flow algorithm of the C_{bank} operated at $PF_{refload}$ of 0.95 lagging.

2.3 Solar PV control

The PF-controlled solar PV system was designed by referring to previous studies [14, 24, 25]. The DC link voltage (V_{dclink}) control was used for improving the system stability. The solar PV system design was based on the DC–DC–AC inverter topology, also known as two-stage power conversion [24]. The DC/DC converter was placed in between the solar PV panel and the DC/AC converter to enhance the design flexibility, voltage gain and energy harvesting capability [24]. A detailed configuration of the PF-controlled solar

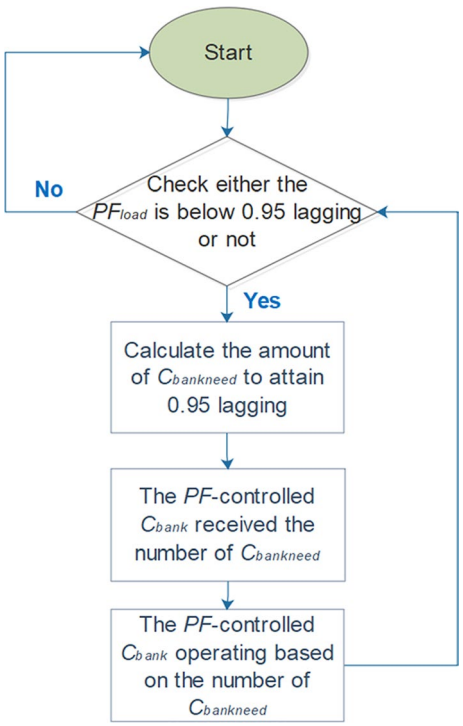

Fig. 2 Flow diagram of the designed C_{bank} operated at $PF_{refload}$ of 0.95 lagging

PV system and the flowchart of the V_{dclink} and PF control process are presented in Figs. 3 and 4, respectively.

The DC/DC converter was installed with a maximum power point tracking (MPPT) device for maximizing the instantaneous DC power output of the solar PV panel. The MPPT device controls the duty ratio of the DC/DC converter (D_{con}) until the DC supply voltage (V_S) of the solar PV panel is reached and maintained at the maximum power point voltage (V_{MPP}) [25]. The best MPPT method for a 400 kW_{pk} solar PV system is the incremental conductance method [25]. The DC link voltage reference ($V_{dclinkref}$) should not be too low and too high, respectively, for an admirable dynamic control and to avoid redundant switching losses [16]. In this case study, the $V_{dclinkref}$ for the solar PV system is permanently set at 950 V. The relationship between the V_S, V_{dclink} and D_{con} is expressed as per mathematical Eq. (1) [16]:

$$V_{\text{dclink}} = -\frac{V_S}{D_{\text{con}} - 1} \tag{1}$$

The V_{dclink} and PF controller was constructed based on the dq control structure due to easy controlling and filtering accomplishment [14]. Based on Figs. 3 and 4, initially, the instantaneous three-phase phase-to-ground voltages (V_{abc}) and three-phase phase-to-ground currents (I_{abc}) output of the solar PV system were obtained by tapping at the AC

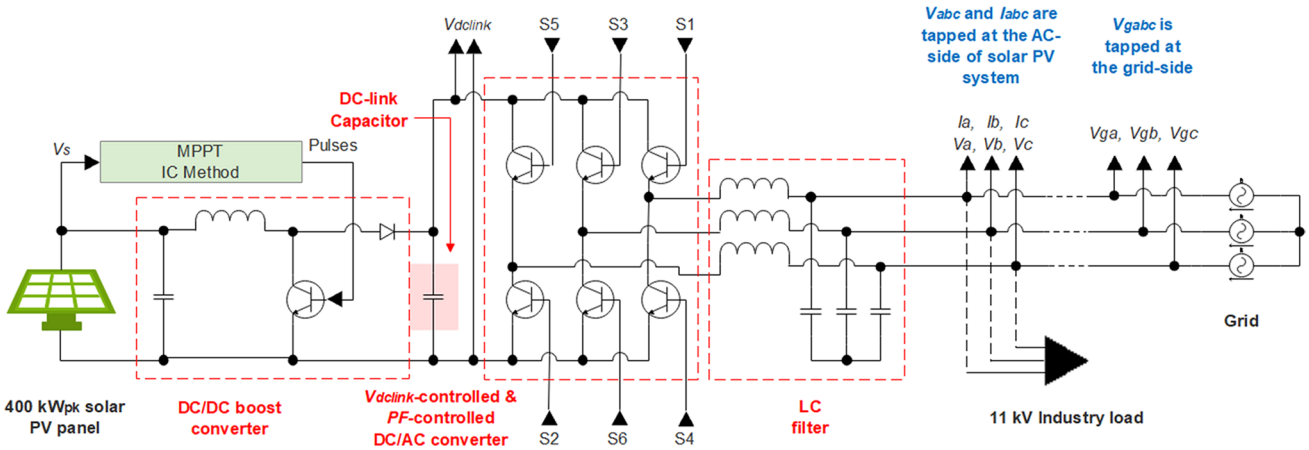

Fig. 3 V_{dclink} and PF control algorithm flow diagram of the designed solar PV system

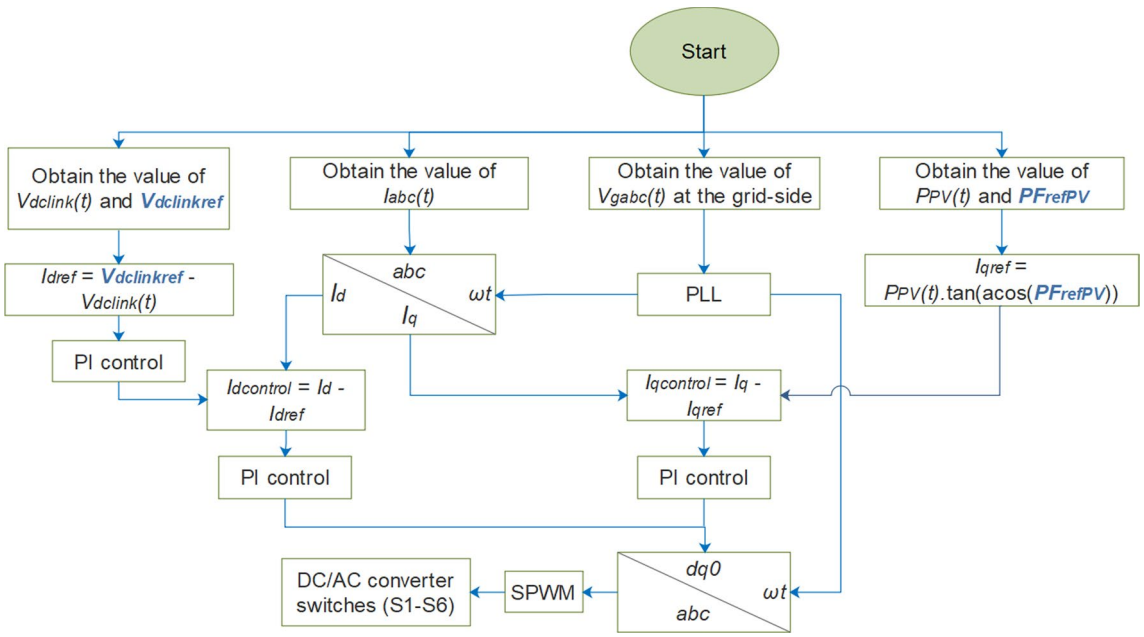

Fig. 4 Detailed control configuration for the designed solar PV system

side after passing the LC filter. The V_{abc} and I_{abc} were converted into a three-phase active power (P_{PV}) form. The P_{PV} and PF_{refPV} then undergo a mathematical transformation to obtain current quadrature reference (I_{qref}).

Meanwhile, the instantaneous three-phase phase-to-ground voltages were obtained at the grid side (V_{gabc}) and sent to the phase-locked loop (PLL) device to get the V_{gabc} phase angle (ωt). In this control system, the PLL device was used for synchronizing the grid phase signal and the solar PV system phase signal [26]. The phase angle was then used in Park and inverse Park transformation. Park transformation is a process of simplifying the fundamental equation, whereas inverse Park transformation is vice versa [27]. In this solar PV system control process, the I_{abc} was simplified to be a direct and quadrature current (I_d and I_q). The instantaneous V_{dclink} was obtained by tapping at the C_{dclink}. It was then compared to the DC link voltage reference ($V_{dclinkref}$) to get the current direct reference (I_{dref}). Next, the I_d and I_q were compared to the I_{dref} and I_{qref}, respectively. The output of these comparisons goes through the PI controller to reduce the offset [28]. It becomes a current direct control ($I_{dcontrol}$) and a current quadrature control ($I_{qcontrol}$) before undergoing the inverse Park transformation and finally, Sine Pulse Width Modulation (SPWM) process. The proportional gain (K_P) value and integral gain (K_I) value of the PI controller were manually tuned based on experiences [28]. Finally, the output of SPWM was fed to the DC/AC converter switches (S1-S6), as shown in Figs. 3 and 4.

The instantaneous PF_{refPV} and the instantaneous P_{PV} will determine the amount of instantaneous Q delivered from the solar PV system (Q_{PV}) to the industrial system. The designed solar PV system has a maximum active power output (P_{maxPV}) of approximately 400 kW. As referred to the guidelines [29], if the P_{PV} is equal or greater than 20% of the DC/AC converter rated power, the PF_{refPV} value should not be lower than 0.9 leading or else the DC/AC converter will get exhausted. So, the PF_{refPV} limit ($PF_{reflimitPV}$) parameter was set at 0.9 leading. The mathematical equation to calculate the amount of Q_{PV} and Q_{maxPV} based on trigonometric power theory is shown in Eq. (2) and (3). Equation (2) indicates that the closer the PF_{refPV} is to unity, the lower the Q_{PV}. The Q_{maxPV} value is vital for C_{dclink} sizing calculation.

$$Q_{PV} = P_{PV}.\tan(\cos^{-1}(PF_{refPV})) \tag{2}$$

$$Q_{\max PV} = P_{\max PV}.\tan(\cos^{-1}\left(PF_{ref\,\lim itPV}\right)) \tag{3}$$

2.4 EV charger control

The designed EV charging system comprises three bidirectional *I*-controlled half-bridge non-isolated DC/DC converter and a V_{dclink} and *PF*-controlled DC/AC converter, as illustrated in Fig. 1. The previous studies [16, 30] are the reference for designing the bidirectional EV charging system. Figure 5 presents a detailed configuration of the designed EV charging system with one charging port.

The V_{dclink} and *PF* control system used in the designed EV charging system is identical to the control system used in the designed solar PV system; thus, the control process is the same as in Fig. 4. The advantages of a bidirectional half-bridge non-isolated DC/DC converter are the high-efficiency, low active component and relatively cost-effective [30]. The *PF* reference for the designed EV charging system (PF_{refEV}) was set to unity. The designed EV charging system can single-charge EV battery with a maximum DC power transfer of 62.5 kW with 125 A of current transfer (I_{EV}) based on CHAdeMO 1.1 standard charging protocol. It can cater simultaneous charge up to three EVs.

The C_{dclink} and LC filter are two vital components in the solar PV and EV charging system. The C_{dclink} is typically utilized to reduce the ripples of V_{dclink} [31] and for providing

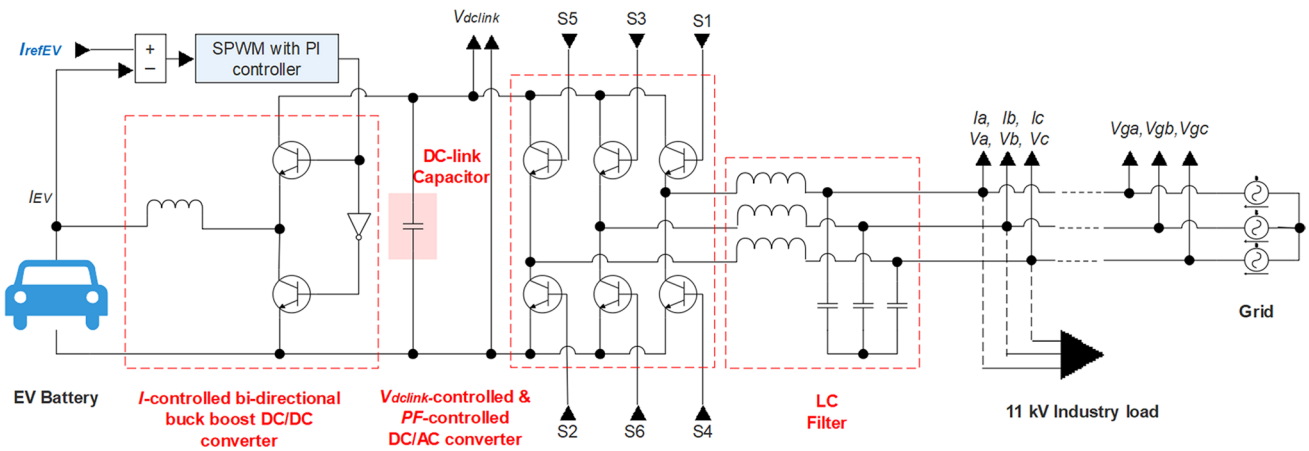

Fig. 5 A detailed configuration of the designed EV charging system

Q support [32]. Oversized and undersized C_{dclink} will result in over expenditure and system failure, respectively. An LC filter is used for smoothening the AC signal [33]. Improper LC filter design will lead to low system power quality.

2.4.1 DC link capacitor modeling

The C_{dclink} is an intermediary electronic component located between the DC/DC converter and the DC/AC converter, as shown in Fig. 1. The Q_{maxPV} is the maximum limit of the amount of Q (Q_{max}) that C_{dclink} can support. The mathematical steps to calculate the sizing of C_{dclink} based on Q_{max} start with the three-phase apparent power (S) equation as per Eq. (4):

$$S = \sqrt{3}VI^* \tag{4}$$

Since only alternating current (AC) is involved, the resistance (R) is replaced with impedance (Z) by using Ohm's law and shown in Eq. (5):

$$V = IZ \tag{5}$$

Substituting Eq. (4) and Eq. (5) gives Eq. (6):

$$S = \frac{\sqrt{3}|V|^2}{Z^*} \tag{6}$$

By considering Q only, the impedance is replaced by capacitor reactance (X_C) as per Eq. (7):

$$Q = \frac{\sqrt{3}|V|^2}{X_C} \tag{7}$$

where Eq. (8) gives X_C:

$$X_C = \frac{1}{2\pi f_s C} \tag{8}$$

Finally, the size of the capacitor (C) in terms of Q_{max} and V_{dclink} derived by Eq. (9):

$$C = \frac{Q_{\max}}{\sqrt{3}.V_{\text{dclink}}^2.2\pi f_s} \tag{9}$$

By considering 25% as a safety margin, the C_{dclink} is assumed to be 25% larger than in Eq. (9). Hence, Eq. (10) established:

$$C_{\text{dclink}} = 1.25C \tag{10}$$

The size of C_{dclink} is measured in Farad (F). The system frequency (f_s) regulated by Malaysian Distribution Code is 50 Hz [34]. Equations (9) and (10) show that a higher Q_{max} consumed larger C_{dclink}, and a higher V_{dclink} will increase C_{dclink}'s Q_{max} support. Table 1 shows the important parameter value used in this PF-controlled solar PV system design.

Table 1 Important parameter's value used for the C_{dclink} sizing in the designed solar PV system

Parameter	Value
System frequency, f_s	50 Hz
Q_{maxPV}	450 kVAr
V_{dclink}	950 V
C_{dclink}	2 mF

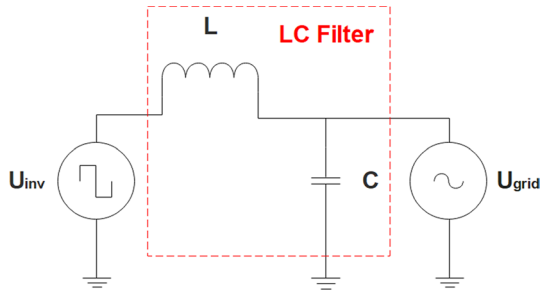

Fig. 6 Basic configuration of an LC filter

2.4.2 LC filter modeling

The LC filter is also known as the low-pass second-order filter. It was installed at the AC side of the designed solar PV system and EV charging system. It can block high-frequency signals and allow only low-frequency signals to pass through it [33]. Figure 6 shows the basic configuration of an LC filter.

The switching frequency (f_{sw}) is 10 kHz. The cut-off frequency (f_c) of the LC filter is the allowable frequency signals upper limit, and it should be less than 1/10$^{\text{th}}$ of f_{sw} [33]. Meanwhile, one research [35] has reported that the f_c value is recommended to be more than 1/14$^{\text{th}}$ of the f_{sw} for less attenuation effect. By considering less attenuation effect and within 0.3% distortion as in IEEE1547 guidelines [35], a mathematical equation for f_c and f_{sw} expressed by Eq. (11):

$$\frac{f_{sw}}{k} < f_c < \frac{1}{10} f_{sw} \; where \; k \simeq 14 \tag{11}$$

As to prevent less than 3% voltage drop across the L_{filter}, the size of L_{filter} is calculated by Eq. (12) [33]:

$$L_{filter} < \frac{0.03U_{inv}}{I_{L\max}(2\pi f_s)} \tag{12}$$

where I_{Lmax} is the maximum RMS load current value, and U_{inv} is the unfiltered output voltage of the DC/AC converter. Finally, the size of C_{filter} is calculated as per Eq. (13) [33]:

$$C_{filter} = \frac{1}{(2\pi f_c)^2 . L_{filter}} \tag{13}$$

Table 2 The parameter's value used to design the LC filter

Component	Value
Switching frequency, f_{sw}	10 kHz
Cutoff frequency, f_c	800 Hz
Inductor, L_{filter}	2 mH
Capacitor, C_{filter}	20 µF

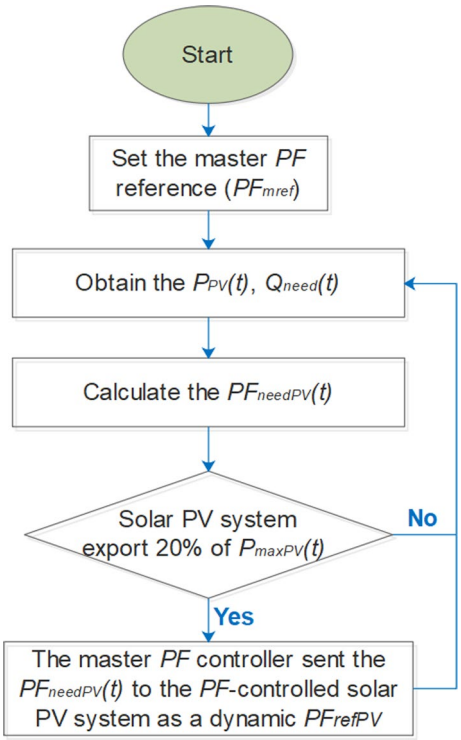

Fig. 7 Flowchart of the control process for the master *PF* controller

Table 2 presents the important parameter's value used in the designed LC filter.

2.5 Master PF control

The proposed master *PF* controller is specialized for regulating the PF_{ind} to attain an intended value by using a single preset reference. The control process is based on the trigonometric power theory calculation. Figure 7 illustrates the flowchart of the master *PF* control process.

The master *PF* reference (PF_{mref}) was preset to 0.95 lagging because of the same reason stated in industrial load's capacitor bank section. The industry's CT and VT sends the total instantaneous currents and voltages received by the industrial system and converted into active power (P_{ind}), reactive power (Q_{ind}) and PF_{ind} forms. The proposed controller had used the PF_{mref}, P_{ind} and Q_{ind} to get the amount of Q needed to achieve PF_{mref} (Q_{need}). Then, the Q_{need} was converted into *PF* form and fed to the *PF*-controlled solar PV system (PF_{needPV}) regarding control of the Q_{PV}. In short, in this master control process, the value of Q_{need} is the same as Q_{PV}. Equations (14) and (15) show the mathematical equations to obtain the Q_{need} and PF_{needPV}.

$$Q_{\text{need}} = Q_{\text{ind}} - P_{\text{ind}}.\tan(\cos^{-1}\left(PF_{\text{mref}}\right)) \tag{14}$$

$$PF_{\text{needPV}} = \cos\left(\tan^{-1}\frac{P_{PV}}{Q_{\text{need}}}\right) \tag{15}$$

3 Results and discussion

The Matrix Laboratory/Simulink software was used to simulate each of the designed equipment. One second in simulation presented as an hour. This section starts with the base case scenario where industrial load without C_{bank}. The industrial load profile was adopted from another study [36]. Figure 8a, b show the simulation result of the power load profile and the instantaneous PF_{ind} before *PF*-controlled C_{bank} was installed, respectively.

Based on Fig. 8a, in a daytime (0700 – 1700), the *P* load reached around 1 MW and 1.2 MW. The daily average of unimproved PF_{load} was nearly 0.8 lagging. The designed *PF*-controlled 600 kVAr C_{bank} then was installed to improve the PF_{ind} within 0.95 lagging. Figure 9a shows the simulation result of the PF_{ind} after installed with the designed *PF*-controlled C_{bank} at 0.95 lagging $PF_{refload}$. The simulation result of the total Q compensated by the *PF*-controlled C_{bank} is shown in Fig. 9b.

Results in Figs. 8a and 9b prove that the PF_{ind} had improved from around 0.8 lagging to nearly 0.95 lagging. In Fig. 9a, the PF_{ind} had experienced slightly over and under correction due to fixed capacitors size [23]. The maximum Q compensated by the C_{bank} was nearly 600 kVAr. Next, the industrial system was connected to the designed *PF*-controlled solar PV system. Figure 10a, b shows the simulation results of the instantaneous power output of the designed solar PV system at unity PF_{refPV}. Figure 10c shows the simulation result of the instantaneous PF_{ind} and $PF_{refload}$ value after the designed solar PV system was installed.

Figure 10b shows that the designed solar PV system started to deliver *P* at the 5th to 19th second (0500 – 1900). It reached P_{maxPV} of approximately 400 kW at 11th second (1100). There was no Q_{PV} because the PF_{refPV} was set at unity. Figure 10c proves the instantaneous PF_{ind} drops drastically after the installation of the solar PV system at unity *PF*. The larger P_{PV} leads to lower PF_{ind}. Hence, this will be a critical case scenario in this case study. Figure 10c also shows that the PF_{ind} was not affected by 0.95 lagging $PF_{refload}$ as the $PF_{refload}$ is only for PF_{load}

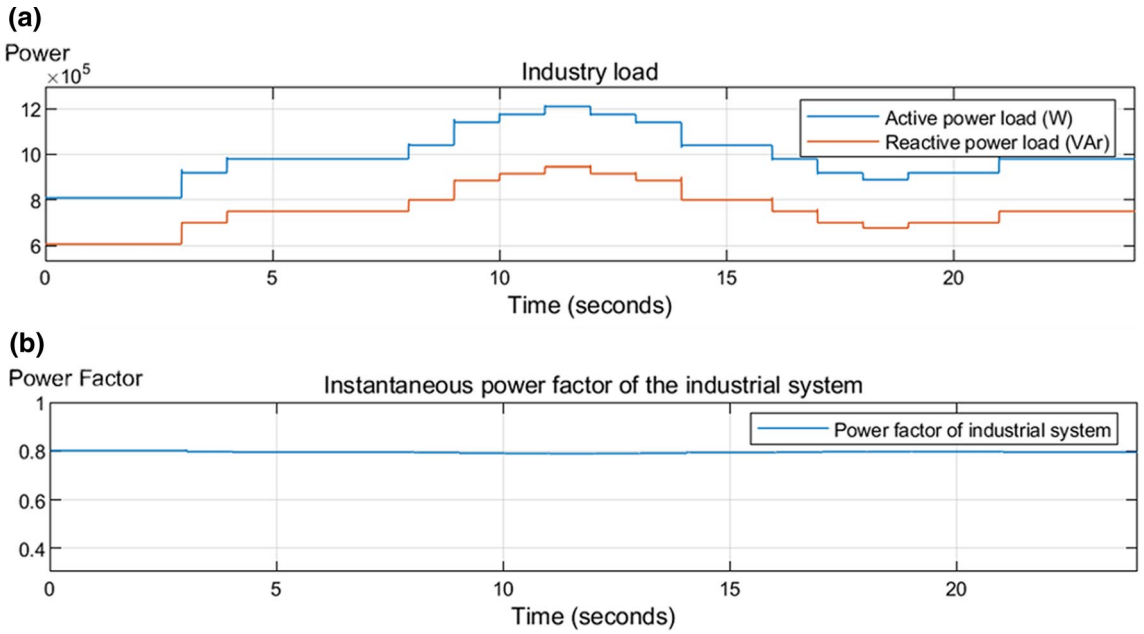

Fig. 8 **a** Load profile of the designed industrial load. **b** Instantaneous PF_{ind} before installed with PF-controlled C_{bank}

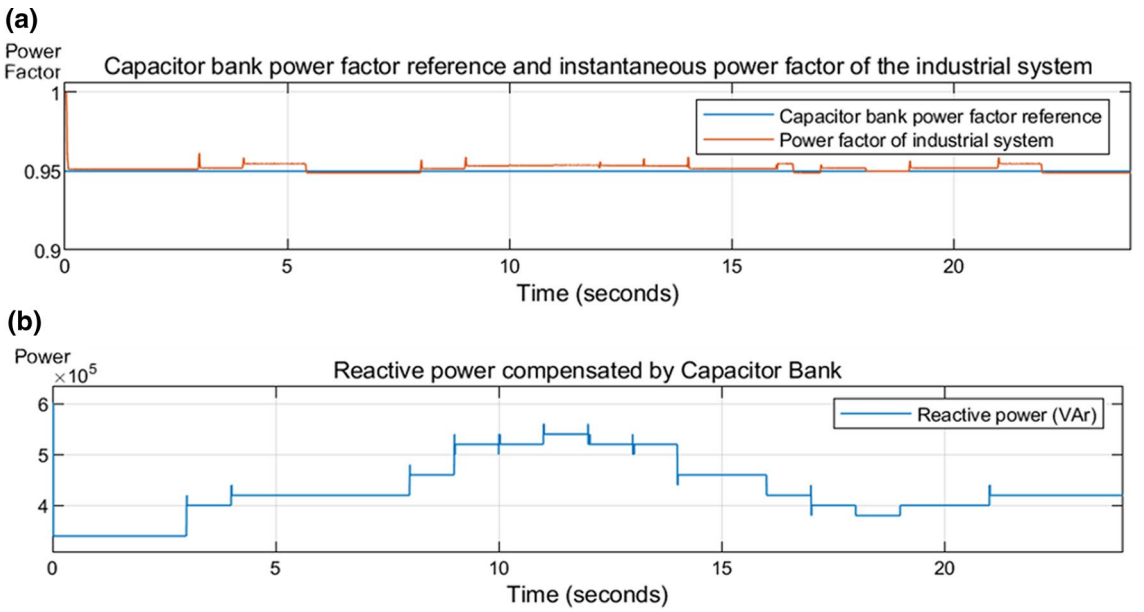

Fig. 9 **a** Instantaneous PF_{ind}, after installed with the designed PF-controlled C_{bank} at 0.95 lagging $PF_{refload}$. **b** The total Q compensated by the PF-controlled C_{bank} at 0.95 lagging $PF_{refload}$

correction. The fluctuations occurred in between the 9th and 13th second are because of the C_{bank} switching alternately on and off [23].

The total harmonic distortion current (THDi) of the solar PV system is measured at the point of common coupling. According to the Energy Commission of Malaysia [29], the THDi percentage for the solar PV system should be less than 5% to avoid low power quality. The mathematical formula to calculate THD_i percentage is given as per Eq. 16 [37]:

$$THD(\%) = 100.\left(\sqrt{\frac{I_2^2 + I_3^2 + I_4^2 + \ldots + I_n^2}{I_1^2}}\right) \tag{16}$$

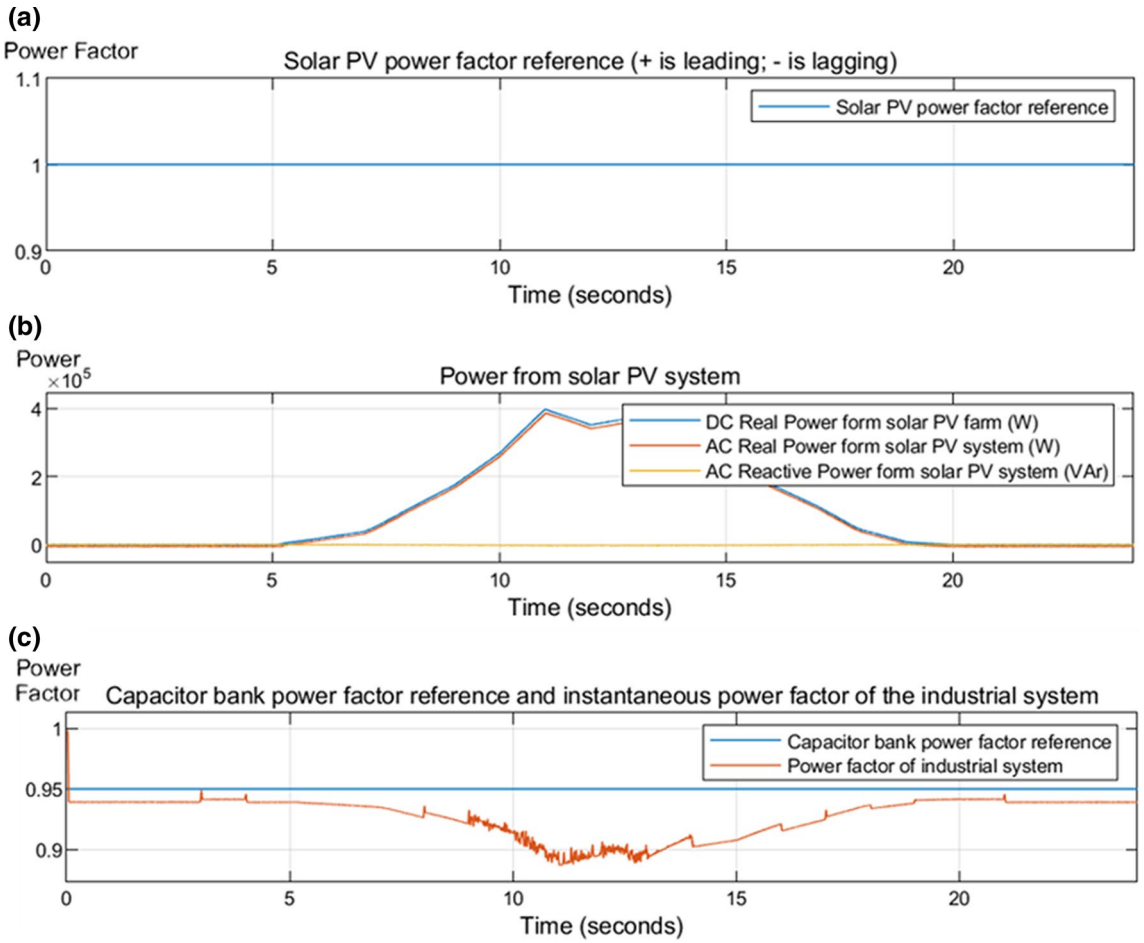

Fig. 10 **a** PF_{refPV} at unity. **b** The instantaneous power output of the designed solar PV system. **c** Instantaneous PF_{ind} and 0.95 lagging $PF_{refload}$

where I_n is the root mean square of the output current and n represents the harmonic number. Figure 11 shows the highest THD_i percentage of the designed solar PV system (4.33%) with its relevant spectrum in a graphical form by using a fast Fourier transform analysis feature in Matrix Laboratory/Simulink software.

The designed EV fast-charging system with three charging ports subsequently had been connected to the industrial system. An EV charging event will slightly increase the PF_{ind}. Figure 12 shows the amount of power transferred to the first, second and third EV. The negative power value indicates the EV in charge mode. There was no Q transfer as the PF_{refEV} is at unity.

Figure 12 illustrates that at the 1st–5th second, the next 6th to 10th second, and the following 11th–15th second, the first, second and third EV is in charge mode, respectively. In the 21st–23rd second, all EVs are simultaneously charged. Thus, this result validates the designed EV charging system can perform a single-charge at nearly 50 kW and can cater a simultaneous charge at almost 150 kW.

Finally, the proposed master PF controller was integrated into the designed industrial system. The PF_{mref} was preset to 0.95 lagging, as shown in Fig. 13c. Figure 13a shows the simulation result of the PF_{needPV} sent from the master PF controller to the solar PV system, which becomes its PF_{refPV}. Figures 13a, b also validates the design of the solar PV system, as per the guidelines [29]. The amount of instantaneous Q_{PV} is related to the instantaneous P_{PV} and the instantaneous PF_{refPV}. Figure 13c shows the simulation result of instantaneous PF_{ind} after the proposed master PF controller was implemented. It shows that the master PF controller is capable of regulating the PF_{ind} to attain 0.95 lagging even though under a critical case scenario.

4 Conclusion

The main contribution of this paper is the design of a master PF controller, which can regulate the PF_{ind} to an intended value by following the PF_{mref}. In this case study, the master

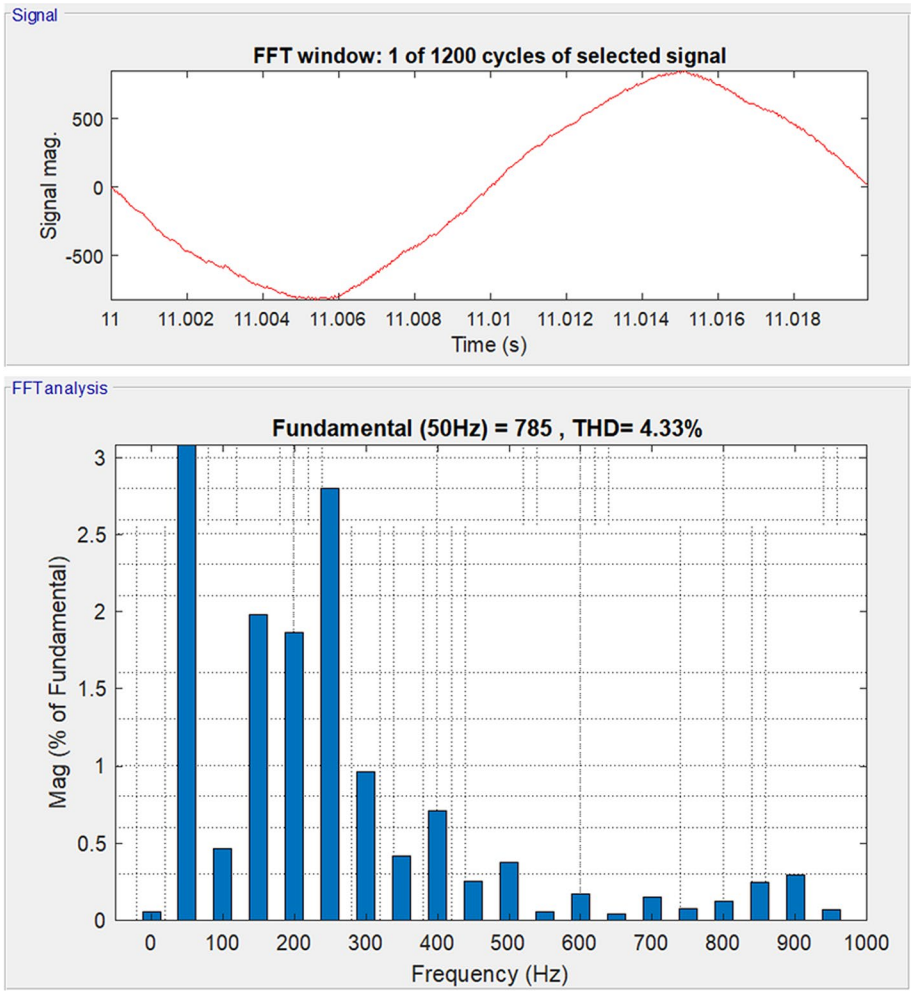

Fig. 11 THD_i percentage of the designed solar PV system and its Fourier spectrum

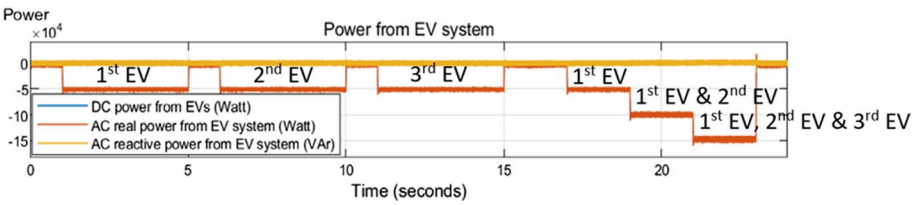

Fig. 12 Three EVs were charging in its time pattern based on the CHAdeMO 1.1 standard charging protocol

PF controller coordinates with the *PF*-controlled solar PV system to perform the PF_{ind} regulation. The proposed master *PF* controller design is simple, correspondingly cost-effective. The mathematical formulas for calculating the sizing of C_{dclink} and LC filter for a solar PV system and EV charging system were also included in this paper. The size of C_{dclink} will determine its *Q* support capability. The LC filter was used instead of L and LCL filters, respectively, because of lesser power losses and cheaper. A bidirectional EV charger was designed in this case study for future research continuation, using the vehicle-to-grid concept. The results and discussion section conclude that the industrial load with a *PF*-controlled C_{bank}, the *PF*-controlled solar PV system, the *I*-controlled EV charging system and the proposed master *PF* controller are able to operate effectively with the proposed control. The proposed master *PF* controller can ensure that the PF_{ind} to be at 0.95 lagging throughout its operation even under a critical case scenario. Hence, these also verify the parameter values used for the C_{dclink} and LC filter.

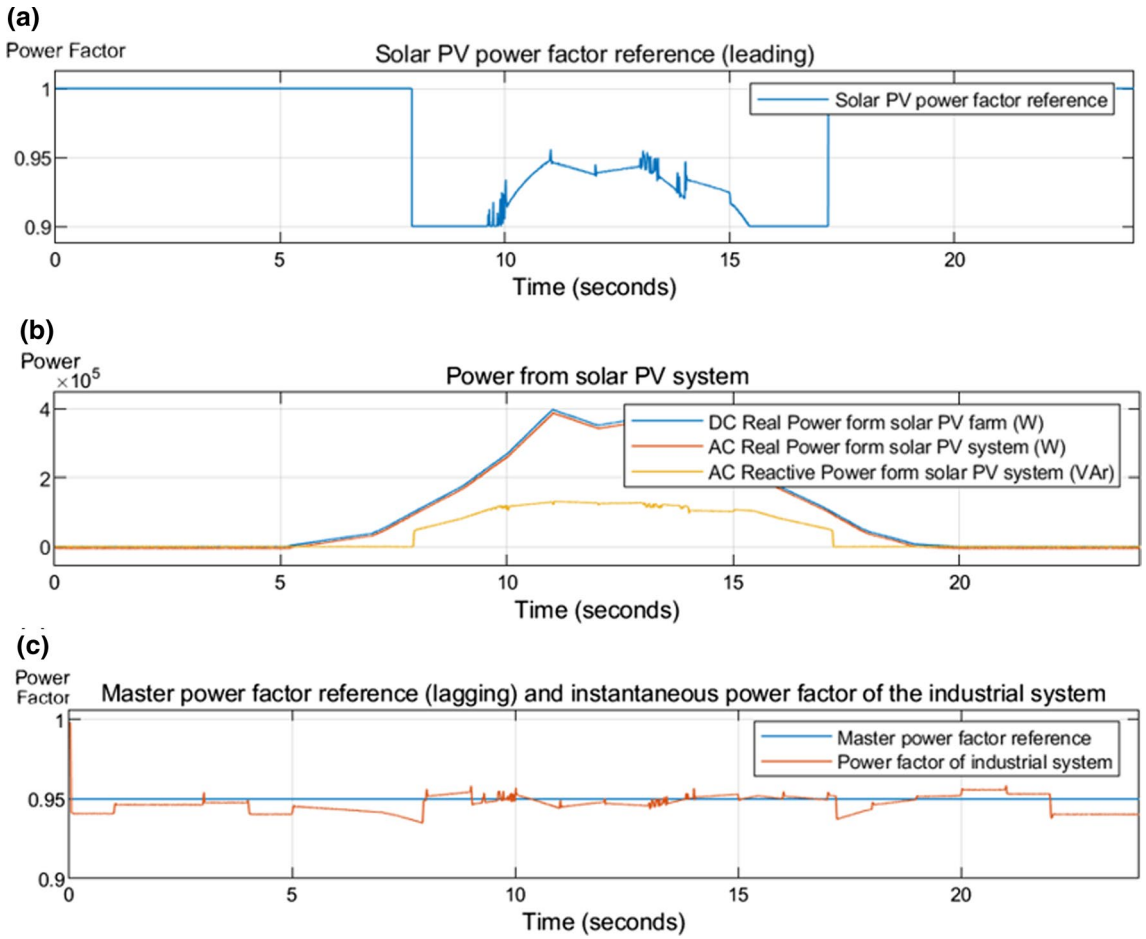

Fig. 13 **a** Instantaneous PF_{refPV}. **b** Instantaneous P_{PV} and Q_{PV}. **c** Instantaneous PF_{ind}, after the proposed master *PF* controller was implemented

Acknowledgements This research was supported by TNB Seeding Project: "Investigation on technical impacts of electric vehicle charging to distribution network."—U-TD-RD-19-29.

Funding This research was supported by the TNB Seeding Project: "Investigation on technical impacts of electric vehicle charging to distribution network."—U-TD-RD-19-29.

Data availability Not applicable.

Compliance with ethical standards

Conflict of interest The authors of this manuscript have no conflict of interest to disclose.

References

1. Kostopoulos E, Spyropoulos G, Kaldellis J (2020) Active-world study for the optimal charging of electric vehicles. Energy Rep 6:418–426. https://doi.org/10.1016/j.egyr.2019.12.008
2. Andreas Radics, Marian Asche (2020) Electric vehicle sales – a global snapshot in uncertain times. Automotive World. https://www.automotiveworld.com/articles/electric-vehicle-sales-a-global-snapshot-in-uncertain-times/. Accessed by 5 May 2020
3. Reshma S, Samuel ER, Unnikrishnan A (2019) A Review of various internal combustion engine and electric propulsion in hybrid electric vehicles. 2nd International Conference on Intelligent Computing, Instrumentation and Control Technologies (ICICICT). Kannur, Kerala, India. pp 316–321. https://doi.org/10.1109/ICICICT46008.2019.8993211
4. Niklas U, von Behren S, Chlond B, Vortisch P (2020) Electric Factor - A comparison of car usage profiles of electric and conventional vehicles by a probabilistic approach. World Electric Vehicle J 11(2):36. https://doi.org/10.3390/wevj11020036
5. Iskandar M, Ariffin A (2019) Relationship between National Automotive Policy (NAP), innovation and automotive vendors'

performance in Malaysia. Manage Sci Lett 9:1181–1198. https://doi.org/10.5267/j.msl.2019.4.022
6. International Energy Agency corporation (2020) Electricity information: overview. International Energy Agency. https://www.iea.org/reports/electricity-information-overview#overview. Accessed by Jul 2020
7. Heymi Bahar (2020) Solar photovoltaic tracking report. International Energy Agency. https://www.iea.org/reports/solar-pv. Accessed by Jun 2020
8. Hidayatno A, Setiawan A, Wikananda Supartha I, Moeis A, Rahman I, Widiono E (2020) Investigating policies on improving household rooftop photovoltaics adoption in Indonesia. Renew Energy 156:731–742. https://doi.org/10.1016/j.renene.2020.04.106
9. Razali A, Abdullah M, Hassan M, Hussin F (2019) Comparison of new and previous net energy metering (NEM) scheme in Malaysia. ELEKTRIKA- Journal of Electrical Engineering. 18(1):36–42. https://doi.org/https://doi.org/10.11113/elektrika.v18n1.141
10. Tenaga Nasional Berhad corporation (2006) Tariff book (Amendments). https://www.tnb.com.my/assets/files/Tariff_booklet.pdf. Accessed 24 May 2006
11. Ciprian MC, Adriana F, Constantin DO (2020) Improving the efficiency and sustainability of power systems using distributed power factor correction methods. MDPI. Sustainability. 12(8). https://doi.org/https://doi.org/10.3390/su12083134
12. Zhou X, Wei K, Ma Y, Gao Z (2020) Review of reactive power compensation device. IEEE International Conference on Mechatronics and Automation (ICMA). Changchun, China. pp 2020–2024. https://doi.org/https://doi.org/10.1109/ICMA.2018.8484519
13. Aziz M, Abdullah A (2020) Hybrid control strategies of SVC for reactive power compensation. Indonesian Journal of Electrical Engineering and Computer Science. 19(2):563–571. https://doi.org/https://doi.org/10.11591/ijeecs.v19.i2.
14. Zeb K, Uddin W, Khan M et al (2018) A comprehensive review on inverter topologies and control strategies for a grid-connected photovoltaic system. Renew Sustain Energy Rev 94:1120–1141. https://doi.org/10.1016/j.rser.2018.06.053
15. Sarkar M, Meegahapola L, Datta M (2018) Reactive power management in renewable rich power grids: a review of grid-codes, renewable generators, support devices, control strategies and optimization algorithms. IEEE Access 6:41458–41489. https://doi.org/10.1109/access.2018.2838563
16. Kang MT, Sanjeevikumar P, Jia YY, Vigna KR (2019) A multi-control vehicle-to-grid charger with bi-directional active and reactive power capabilities for power grid support. Energy 171:1150–1163. https://doi.org/10.1016/j.energy.2019.01.053
17. Tenaga Nasional Berhad corporation (2019) Electricity supply application handbook (Amendments). https://www.tnb.com.my/assets/files/2020.04.14_ESAH_3.1.pdf. Accessed on 11 Nov 2019
18. Nissan corporation (2019) Nissan lead 2019 brochure. https://www.nissan.com.my/vehicles/all-new-nissan-leaf/overview. Accessed on 2 Nov 2019
19. Habib S, Khan MM, Hashmi K, Ali M, Tang H (2017) A comparative study of electric vehicles concerning charging infrastructure and power levels. International Conference on Frontiers of Information Technology (FIT). pp 327–332. https://doi.org/https://doi.org/10.1109/FIT.2017.00065
20. Fuad M (2007) Power factor correction and power quality issues. JURUTERA article. pp 42–45.
21. Joksimovic G (2014) Transformer reactive power compensation – fixed capacitor bank calculation. IEEE Transaction on Power Delivery. 30(99). https://doi.org/https://doi.org/10.1109/TPWRD.2014.2373039
22. Soe Win Naing (2017) Application of distribution system automatic capacitor banks for power factor improvement (132/66/33 kV, 90 MVA Aung Chan Thar (Monywa) Substation in Myanmar). American Journal of Science, Engineering and Technology. 2(4):120–131. https://doi.org/https://doi.org/10.11648/j/ajset20170204.14
23. Moein A, Mahdi D, Amir S, Firouz BA (2020) Shunt capacitor bank: Transient issues and analytical solutions. Elsevier. International Journal of Electrical Power and Energy Systems. 120:106025. https://doi.org/https://doi.org/10.1016/j.ijepes.2020.106025
24. Raveendhra D, Pathak MK (2019) Recent trends in solar PV inverter topologies. Elsevier Solar Energy 183:57–73. https://doi.org/10.1016/j.solener.2019.02.065
25. Riaz A, Ali FM, Hadeed AS (2019) Power tracking techniques for efficient operation of photovoltaic array in solar applications – a review. Renew Sustain Energy Rev 101:82–102. https://doi.org/10.1016/j.rser.2018.10.015
26. Golestan S, Guerrero JM, Vasquez JC (2017) Three-phase PLLs: a review of recent advances. IEEE Trans Power Electron 32:1894–1907. https://doi.org/10.1109/TPEL.2016.2565642
27. Jayarama P, Rajagopalan D (2015) Adoption of Park's transformation for inverter fed drive. Int J Power Electron Drive Syst, 5(3):366–373. https://doi.org/https://doi.org/10.11591/ijpeds.v5i3.6849
28. Shri B, Anil K, Soni JS (2016) A review on: PID controller. International Journal on Recent Technologies in Mechanical and Electrical Engineering (IJRMEE). 3(2):17–22. http://www.ijrmee.org/download/browse/Volume_3_Issues/February_16_Volume_3_Issue_2/1457198099_05-03-2016.pdf. Accessed on 3 Mar 2016
29. Suruhanjaya Tenaga Corporation (2015) Guidelines for solar photovoltaic installation on net energy metering system. Electricity Supply Act (Amendment).
30. Omer T, Unal Y, Ahmet T (2018) Overview of battery charger topologies in plug-in electric vehicle and hybrid electric vehicle. 16th International Conference on Clean Energy (ICCE). https://www.researchgate.net/publication/327422059_OVERVIEW_OF_BATTERY_CHARGER_TOPOLOGIES_IN_PLUG-IN_ELECTRIC_AND_HYBRID_ELECTRIC_VEHICLES. Accessed on 4 Sep 2018
31. Hyo-Cul I, Seok-Min K, Kyo-Beum L (2018) Design and control of small DC-link capacitor-based three-level inverter with neutral-point voltage balancing. MDPI Energies 11(6):1435. https://doi.org/10.3390/en11061435
32. Jia YY, Seyed MF, Vigna KR, Kang MT (2017) Design and development of a three-phase off-board electric vehicle charger prototype for power grid voltage regulation. Energy 133:128–141. https://doi.org/10.1016/j.energy.2017.05.108
33. Mojgan H, Mehrdad H (2015) Design, application and comparison of passive filters for three-phase grid-connected renewable energy systems. ARPN J Eng Appl Sci 10(14):10691–10697
34. Suruhanjaya Tenaga corporation (2017) Distribution code for peninsular malaysia, sabah & f.t. labuan (amendments) 2017. Suruhanjaya Tenaga. https://www.st.gov.my/en/general/add_counter/605/download/read_count. Accessed on 11 Apr 2017
35. Pritha R, Jitendra NB, Gautam S, Sumana C (2018) Performance evaluation and filter design aspects of single-phase inverter under different loading conditions. IETE J Res 66(1):103–114. https://doi.org/10.1080/03772063.2018.1466734
36. Carpinelli G, Khormali S, Mottola F, Proto D (2014) Battery energy storage sizing when time of use pricing is applied. Sci World J 2014:1–8. https://doi.org/10.1155/2014/906284
37. Liqaa A, Jiashen T (2019) Advances in reduction of total harmonic distortion in solar photovoltaic systems: a literature review. Int J Energy Res 44(4):1–16. https://doi.org/10.1002/er.5075